CrossMark

Optimization of Cu_2ZnSnS_4 thin film absorber layer growth without sulphurization using triethanolamine as complexing agent for thin film solar cells applications

J. J. Chaudhari[1] · U. S. Joshi[1]

Abstract

Quaternary kesterite Cu_2ZnSnS_4 (CZTS) thin films have been prepared via a simple spin-coating technique based on a sol–gel precursor of 2-methoxyethanol solution with metal salts and thiourea. Solution processed CZTS thin film growth parameters using complexing agent triethanolamine (TEA) have been investigated. Effects of complexing agent TEA on structural, morphological, optical, electrical and photovoltaic properties of CZTS thin films were systematically investigated. X-ray diffraction and Raman spectroscopy studies reveal that amorphous nature of CZTS thin film changes into polycrystalline with kesterite crystal structure with optimized TEA concentartion. Surface morphology of CZTS films were analyzed by field emission scanning electron microscope and atomic force microscope, which revealed the smooth, uniform, homogeneous and densely packed grains and systematic grain growth formation with varying TEA concentrations. UV–Vis spectra revealed a direct energy band gap ranging from 1.78 to 1.50 eV, which was found to depend upon the TEA concentration. X-ray photoelectron spectroscopy demonstrated stoichiometric atomic ratios of multicationic quaternary CZTS thin film grown without sulphurization. p-type conductivity was confirmed using Hall measurements and the effect of varying concentartion of TEA on electrical and photovoltaic properties are studied. The SLG/FTO/ZnO/CZTS/Al thin film solar cell is fabricated with the CZTS absorber layer grown at optimized TAE concentration of 0.06 M. It shows a power conversion efficiency of 0.87% for a 0.16 cm^2 area with V_{oc} = 0.257 mV, J_{sc} = 8.95 mA/cm^2 and FF = 38%.

1 Introduction

With constant rising concerns regarding global warming and increase in worldwide energy demand, clean renewable energy is ultimate solution for our future energy needs. Among all renewable energy sources, solar energy is extremely promising, abundant and clean energy source. However, the scope of large scale photovoltaic energy production from solar energy by utilizing earth abundant, non-toxic and environment friendly materials is consider as a pressing issue in photovoltaics. Recently, thin film solar cell (TFSC) based on $Cu(In,Ga)Se_2$ (CIGS) absorber layer have gained a remarkable attention in photovoltaic market. Highest efficiency achieved by CIGS solar cell is about 21.7% [1]. However, CIGS solar cell contains expensive and rare metals such as gallium and indium, which affects large scale fabrication of CIGS solar modules at low cost. Therefore, large scale fabrication of TFSCs requires appropriate alternate materials that are abundantly available in the earth's crust and environmentally friendly. Chalcogenide materials such as Cu_2ZnSnS_4 (CZTS), $Cu_2ZnSnSe_4$, and Cu_2CdSnS_4 are promising materials and have similar crystal structure and electronic properties to that of CIGS. Among them, CZTS thin films are one of the most promising materials for fabrication of low cost TFSCs since they consist of earth abundant materials. CZTS is a quaternary p-type semiconducting material with direct energy band gap in the range 1.0–1.6 eV and high optical absorption coefficient of above 10^4 cm^{-1} [2].

CZTS thin films can be synthesized by pulse laser deposition with conversion efficiency of 4.13% [3], co-sputtering with conversion efficiency of 6.77% [4], and fast co-evaporation technique with conversion efficiency of 4.1% [5]. These methods are relatively costly because ultra high vacuum is essentially required in these methods. Also, there are low cost solution deposition methods like sol–gel with

✉ J. J. Chaudhari
  jigarchaudhary08@gmail.com

[1] Department of Physics, School of Sciences, Gujarat University, Ahmedabad 380009, India

conversion efficiency of 0.63% [6], sol–gel sulfurization with conversion efficiency of 1.01% [7], spray pyrolysis with conversion efficiency of 1.4% [8] which can be utilized to fabricate CZTS thin films.

In this study, we developed non-toxic solvent based technique of fabricating CZTS thin films without sulphurizarion process. We have synthesized stoichiometric CZTS thin films with a kesterite crystal structure from non-toxic solvent 2-methoxyethanol by sol–gel technique [9]. As an environmentally benign solvent, 2-methoxyethanol was selected because it can evaporate rapidly and thus may minimize any residual of carbon or oxygen containing impurities in the CZTS thin film. Mitzi and co-authors synthesized $Cu_2ZnSn(S,Se)_4$ solar cell and demonstrated high conversion efficiency of 9.6% [10]. Though the solar cells demonstrated the promising and high power conversion efficiency, this method utilized hydrazine hydrate, which is a highly toxic and flammable solvent. Furthermore, Ki and Hillhouse synthesized CZTS solar cell with conversion efficiency of 4.1% [11] using toxic dimethyl sulfoxide as a solvent and CZTS thin films were annealed at high temperature up to 550 °C. In addition, Jiang et al. [6] fabricated CZTS films with large and densely packed grains demonstrating conversion efficiency of 0.63%. Though this method showed simple technique to fabricate high crystalline CZTS thin film preparation, the method utilized hydrogen sulfide (H_2S) gas to compensate loss of volatile sulphur and reduce oxide formation during the annealing process. Here, we have utilized thiourea as a source of sulphur that can readily form complexes with copper, zinc and tin. In addition, we have studied the influence of complexing agent triethanolamine (TEA) on thin films. TEA is a complexing agent that determines the structural, morphology, electrical and photovoltaic properties of thin film. Our results reveal that different concentration of TEA has significant effects on photovoltaic properties of CZTS thin films.

2 Experimental procedure

The CZTS precursor solutions were prepared by dissolving copper (II) chloride $CuCl_2 \cdot 2H_2O$ (0.01 M), zinc (II) chloride $ZnCl_2 \cdot 2H_2O$ (0.005 M), tin (II) chloride $SnCl_2 \cdot 2H_2O$ (0.005 M) and thiourea NH_2CSNH_2 (0.05 M) in 10 ml 2-methoxyethanol. Molar ratio of precursors Cu/Zn/Sn/S of 2:1:1:5 was used. Excess amount of thiourea was required to avoid secondary sulphide phases and precipitation of metal sulfides and hydroxides since thiourea makes complexes with metal hydroxide and sulfide [12]. TEA was used as a complexing agent and molar concentrations of TEA in the precursor solutions were varied as 0, 0.02, 0.04 and 0.06 M. TEA were added in precursor solutions before adding thiourea. Crystal clear, bright yellow colored and homogeneous sol–gel solutions were formed by stirring precursor solutions at 60 °C for 40 min after complete dissolution of all chemicals.

Glass substrates (2.5×2.5 cm^2) were cleaned with detergent solution and distilled water and then sonicated in the mixture of isopropyl alcohol and acetone (1:1) for 15 min. After that, RCA cleaning of glass substrates were done in the mixture of ($NH_4OH + H_2O_2 +$ distilled water) (1:1:5) at 85 °C for 15 min. To prepare thin films of CZTS, precursor solutions with different concentration of TEA were spin coated on cleaned glass substrates at 2000 rpm for 25 s (Apex Instruments, model SCU 2005). Glass substrates were termed as CZTS-0, CZTS-1, CZTS-2, and CZTS-3 corresponding to the concentration of TEA of 0, 0.02, 0.04 and 0.06 M respectively. The precursor layers were then dried on a hot plate in air at 200 °C for 30 min to remove any residue of organic solvent. The process of coating and drying of thin films was repeated until desired thickness was obtained. The as-grown films were then annealed in an argon atmosphere at 450 °C for 1 h.

The crystallographic phase of CZTS thin films were observed by using X-ray diffractometer (BRUKER D2 PHASER) using CuKα radiation ($\lambda = 1.5418$ Å). To confirm formation of single phse Kesterite CZTS structure, Raman shift spectra of CZTS thin films were executed by Renishaw InVia Raman microscope with an excitation wavelength of 514.5 nm by argon–ion laser at 50 mW power. Surface morphology was studied by atomic force microscopy (AFM) (Nanosurf Easyscan 2, Nanosurf). The surface and cross-sectional view of CZTS films were analyzed by field emission scanning electron microscope (FE-SEM Carl ZEISS GeminiSEM 500). Charge carrier concentration in CZTS thin films were estimated by Hall measurements (HMS-3000, Ecopia Corp.). Optical properties of CZTS films were studied by UV–Vis spectrophotometer (Shimadzu UV-2600). The elemental composition analysis in CZTS thin films was analyzed by X-ray photoelectron spectrometer. An Mg Kα (1253.6 eV) source and a DESA-150 electron analyzer (Staib instruments, Germany) were utilized to record the X-ray photoelectron spectroscopy (XPS) spectra. The J–V characteristics of CZTS TFSCs were measured in illumination condition using a source-measurement unit (U2722A, Agilent) combination with a class AAA solar stimulator (SS50AAA, Photo Emission Tech., Inc.) with a simulated AM 1.5 G spectrum and power density of 100 mW/cm^2 at 25 °C.

3 Results and discussion

3.1 Structure properties

In order to explain the effect of TEA concentration on the structure properties of CZTS thin films, the CZTS precursor

thin films were deposited without and with TEA as a complexing agent ranging from 0, 0.02, 0.04 and 0.06 M concentrations. Figure 1 presents the X-ray diffraction (XRD) patterns of CZTS thin films deposited with different concentration of TEA. The XRD of CZTS thin films indicate sharp peak at 2θ values of 28.5°, 33.0°, 47.3° and 56.3°, which are identified due to reflection from (112), (200), (220) and (312) planes of CZTS thin films. XRD peaks of CZTS (JCPDS 26-0575) at 28.5°, 33.0°, 47.3°, and 56.3° confirm single phase kesterite CZTS [13]. It can be seen that CZTS thin film deposited without complexing agent TEA indicates very weak and less intense diffraction peaks as compared with the addition of complexing agent. It shows that crystallinity of the kesterite phase in the CZTS thin films is improved with complexing agent. We did not observe XRD peaks of several related sulfides such as CuS, ZnS and Cu_2SnS_3, which may present in the growth of CZTS thin films. These results revealed that the concentration of TEA affects crystal structure and phase purity of CZTS films as can be seen in Fig. 1. A relatively more intense and sharper (112), (200), (220) and (312) diffraction peaks are observed for the CZTS thin film deposited with 0.06 M TEA. From the XRD peaks, the crystallite size of CZTS thin films can be estimated by Scherrer's formula [14].

$$t = \frac{0.9\ \lambda}{\beta\ \cos\theta}$$

where t is mean crystallite size (nm), λ is wavelength of X-ray (Cu Kα) and its value is 1.5418 Å, β is broadening at half maximum intensity, θ is Bragg angle.

Maximum strain (ε) in the CZTS films deposited without and with complexing agent TEA was determined by formula [14].
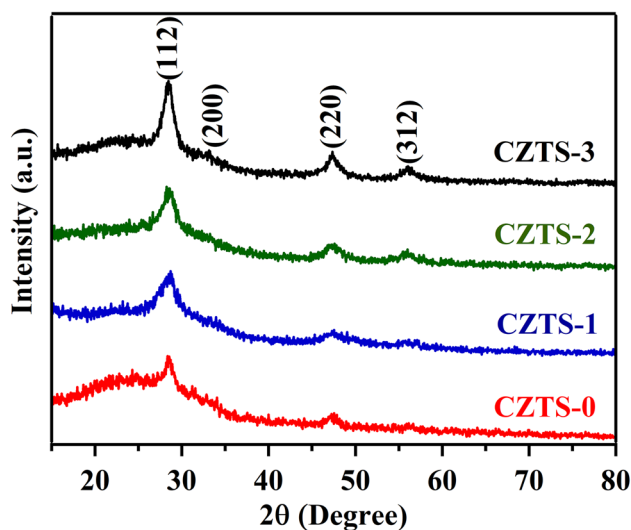
$$\varepsilon = \frac{\beta \cot \theta}{4}$$

The variation of crystallite size with variation of concentration of complexing agent is shown in Table 1. Based on Scherrer's formula the average crystallite size of four samples (i.e. CZTS-0, CZTS-1, CZTS-2 and CZTS-3) are as shown in Table 1, the crystallite size of the CZTS films increases with increase in concentration of complexing agent from 0 to 0.06 M. Thus, CZTS thin films with higher concentration of complexing agent may have bigger crystallite size. As a result, it can be summarized that, complexing agent in the precursor solutions affects the crystal structure and phase purity of CZTS thin films. Moreover, strain of CZTS films decreases with increase in concentration of complexing agent, which leads to increase in the crystallite size of CZTS thin films [15].

It may be noted that the crystal structure of CZTS thin film is similar to zinc-blend type structure, like binary sulfide Cu_2S, ZnS, SnS_2 and ternary sulphide Cu_2SnS_3. Because of similar lattice parameters, the XRD measurements of CZTS thin films solely cannot confirm the formation of single phase kesterite CZTS structure [16–18]. Therefore, Raman spectroscopy was performed to confirm the existence of any secondary phases in the CZTS thin films. XRD results confirmed that there were no secondary phases in all CZTS thin films apart from single phase kesterite CZTS. Thereby, one cannot expect major difference in Raman analysis too. Hence, a Raman measurement of only CZTS-0 and CZTS-3 thin films was investigated. Figure 2 shows Raman shift spectra ranging from 200 to 500 (cm^{-1}) of CZTS-0 and CZTS-3 thin films. Raman spectroscopy is an optical technique where interaction volume in the thin film samples depends on excitation wavelength, absorption coefficient and the energy band gap [19, 20]. Therefore, selection of appropriate laser source with required excitation wavelength is essential [19]. Hence, Raman measurement of both CZTS thin films was done by excitation wavelength of 514.5 nm by argon–ion laser at 50 mW power. The Raman shift spectra indicate two distinct Raman modes; main strong peak at around 335 cm^{-1} and weak peak at around 288 cm^{-1}. These Raman peaks are due to single phase kesterite CZTS structure in both CZTS thin films and these peaks are in good

Fig. 1 XRD patterns of CZTS thin films prepared without and with different concentrations of TEA

Table 1 Crystallite size and maximum strain in CZTS thin films with different concentration of TEA

Sample name	Concentration of TEA (M)	Crystallite size (XRD) (nm)	Max. strain (%)
CZTS-0	0	10.49	10.32
CZTS-1	0.02	15.34	8.69
CZTS-2	0.04	19.42	7.01
CZTS-3	0.06	28.16	5.16
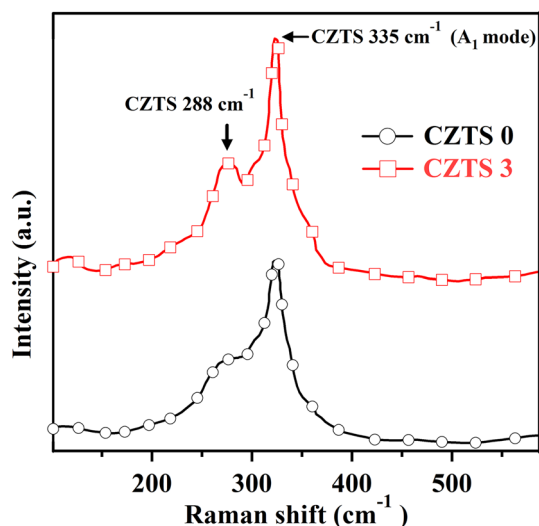
Fig. 2 Raman shift spectra of CZTS-0 and CZTS-3 thin film samples

Fig. 3 $(\alpha h\upsilon)^2$ versus photon energy ($h\upsilon$) plot of CZTS thin films fabricated with different amounts of TEA for determination of energy band gap

agreement with reported Raman spectra of CZTS [21, 22]. The main peak at 335 cm^{-1} is due to the A$_1$ vibration mode, arising from vibration of S atoms in kesterite CZTS lattice while other atoms remain stationary at their positions [23]. The weaker peak at 288 cm^{-1} was determined by polarization dependent Raman spectroscopy using selection rules and it arises due to B (TO LO)/E (TO LO) modes [24]. The full width at half maximum (FWHM) of the A$_1$ vibration mode of CZTS-3 thin film at 335 cm^{-1} is more intense compared to the A$_1$ mode of CZTS-0 thin film. The variation of FWHM of A$_1$ vibration mode shows variation in average particles size in CZTS thin films [25]. The main Raman peaks become strong and narrow with increasing concentration of complexing agent up to 0.06 M suggesting good crystallinity of CZTS-3 thin film [25]. Moreover, no noticeable Raman peaks corresponds to Cu$_2$SnS$_3$ [26, 27], ZnS [28], Cu$_{2-x}$S [29] and/or S$_n$S [30] are present in the spectra. These results clearly indicate the growth of single phase kesterite CZTS structure even at low processing temperatures [31]. Combined XRD and Raman spectroscopy results confirm a phase pure CZTS growth arising due to optimal concentration of complexing agent even on glass substrates at low temperature of 450 °C and with non-vacuum process.

3.2 Optical properties

Optical properties of CZTS thin films were analyzed by using UV–Vis spectroscopy. Optical energy band gap of CZTS thin films were calculated by Tauc relation [32] for direct energy band gap semiconductor,
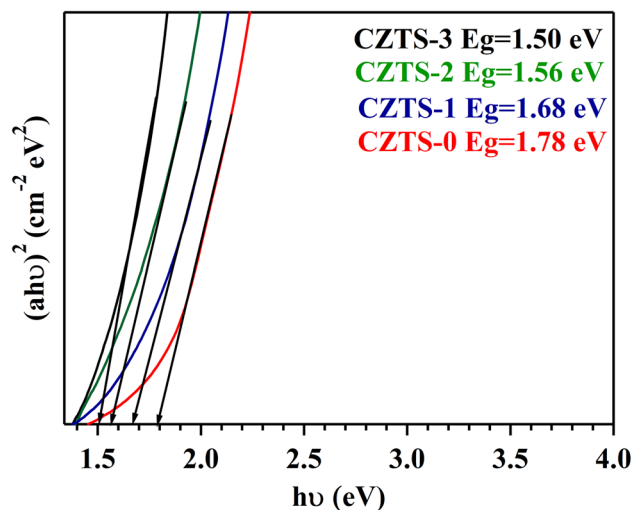
$$\alpha h\upsilon = B\left(h\upsilon - E_g\right)^n$$

where α is absorption coefficient in (cm^{-1}), h is plank constant in (Js), υ is the frequency of radiation (Hz), B is proportionality factor called Tauc parameter, E$_g$ is the optical energy band gap (eV), n is the parameter connected with distribution of density of states and its value is ½ for allowed direct energy band gap.

As shown in Fig. 3, the optical band gap energy is estimated by extrapolating the linear region in the $(\alpha h\upsilon)^2$ plot and determining its intercept with photon energy ($h\upsilon$) axis. As shown in Fig. 3, there is significant effect of complexing agent on energy band gap of CZTS thin films. CZTS-0 thin film deposited without complexing agent has the highest energy band gap of 1.78 eV, whereas, CZTS film (CZTS-1) deposited with higher concentration of TEA 0.02 M has energy band gap of 1.68 eV and CZTS-2, CZTS-3 films deposited with 0.04 and 0.06 M of TEA; demonstrate decreasing order of energy band gap of 1.56 and 1.50 eV, respectively. The UV–Vis spectra of CZTS thin films are in good agreement with previously reported literature results for CZTS [33]. This reveals that band gap of CZTS decreases with systematic increasing concentration of complexing agent. The energy band gap of CZTS thin films varies from 1.78 to 1.50 eV. These are appropriate values of band gap for application of CZTS absorber layer in TFSCs applications. Such a decreasing order in band gap is observed due to various factors like lattice strain and crystallite size in CZTS lattice [34]. Further, the decrease in the energy band gap with increasing concentration of complexing agent is also attributed to decrease in the lattice defects and improved crystallinity of CZTS thin films. Therefore, the probability of electron scattering at grain boundaries (GBs) decreases, consequently, transition of electrons from valance band to

conduction band may become easy; signifying a decrease of energy band gap.

3.3 Surface morphology

Surface morphology of CZTS thin films was investigated by using AFM. Figure 4 shows two-dimensional AFM images and size distributions of CZTS thin films with different concentrations of complexing agent. As shown in Fig. 4, AFM images indicate that CZTS thin films have homogeneous grains distribution for all the thin films with varying concentration of complexing agent. As CZTS thin film is used as an absorber layer of TFSC, grains of CZTS thin film should be uniform, nano sized and densely packed [35]. Smooth surface of CZTS thin film is advantageous to decrease the dark current in the thin film photovoltaic device and it also decreases number of interface states between absorber layer and window layer [36]. The effect of concentration of complexing agent on CZTS grain growth is evident in the AFM images of Fig. 4a, c, e and g, where a systematic increase in the average grain size is seen. Figure 4b, d, f and h shows histograms of crystallite size distribution in the CZTS thin films deposited with different concentration of complexing agent. Histogram images reveal that crystallite size distribution of CZTS thin films is very sharp indicating that the films possess mono-dispersed grain distribution in CZTS thin films. Analysis of concentration of complexing agent on surface morphology is summarized in Table 2. It is observed that RMS roughness increases notably with increase of the concentration of TEA [15]. Here, complexing agent TEA makes complexes with free cations and forms Cu–TEA, Zn–TEA, Sn–TEA complexes rather than free metal cations as in case of the absence of TEA, and complex decomposition mechanism fabricates nano structure CZTS. Cu–TEA, Zn–TEA and Sn–TEA complexes decomposed during the annealing process and forms kesterite CZTS. Here, complexing agent improves nano structure and grain growth in CZTS thin films. As size of the grain in CZTS thin film increases GB decreases, which increases effective diffusion length of minority charge carrier and increases short circuit current density. The efficiency of TFSC can be enhanced by increasing size of the grains in absorber layer, and therefore larger gains are beneficial to improve conversion efficiency of TFSCs device. The size of the grains of CZTS thin films is an important factor to determine the efficiency of TFSC. Larger grain size improves charge transport mechanism in comparison to small grain sized CZTS thin films [37]. Figure 5 displays the dependence of RMS roughness and crystallite size of CZTS thin films on concentration of complexing agent in the CZTS film growth. Analysis of Fig. 5 suggest that CZTS-0 film deposited without complexing agent has small grain and less value of RMS roughness, i.e., it possesses the smoothest surface, while CZTS thin films
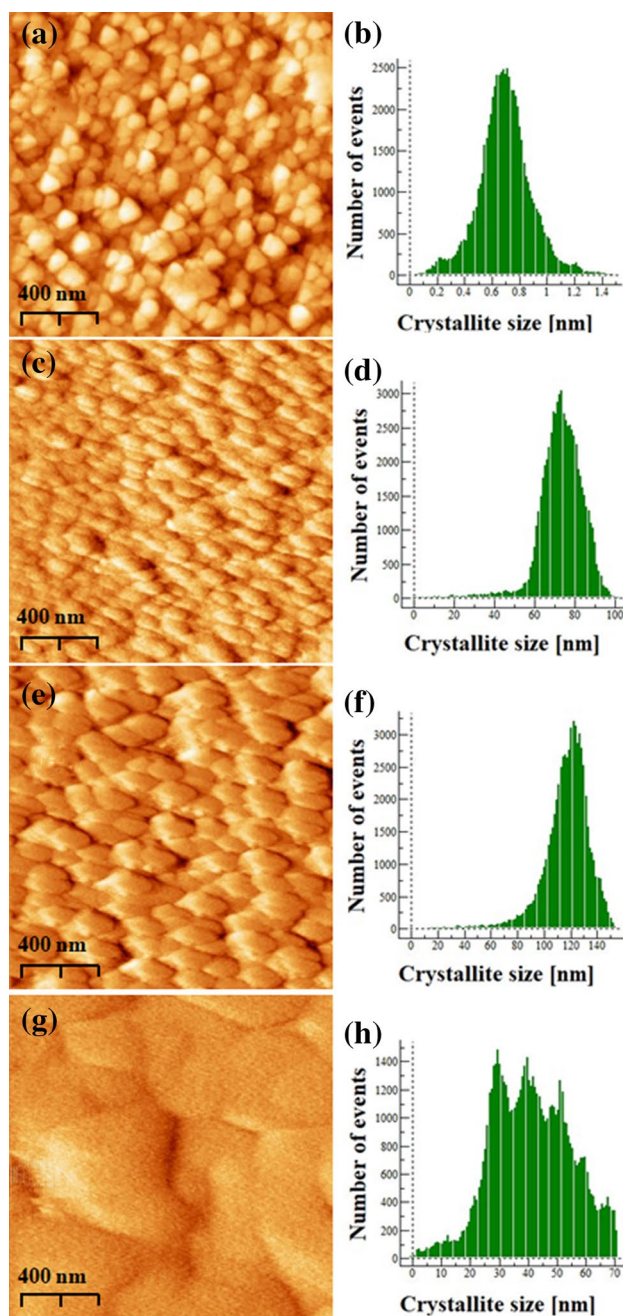

Fig. 4 Two-dimensional AFM images and size distribution histograms of **a, b** CZTS-0, **c, d** CZTS-1, **e, f** CZTS-2, **g, h** CZTS-3 thin film samples

deposited with increasing concentration of complexing agent have large grain size and increasing order of RMS roughness. An improvement in crystallinity of CZTS thin films with increase in concentration of TEA is due to the ability of adatoms to move towards stable site in CZTS lattice, therefore favouring grain growth in CZTS thin films. Moreover, Cu–TEA, Zn–TEA, Sn–TEA complexes which decomposed to form CZTS thin film are responsible for higher grain size

Table 2 RMS roughness of CZTS thin films deposited with different concentration of TEA

Sample name	Concentration of TEA (M)	RMS roughness (nm)
CZTS-0	0	1.85
CZTS-1	0.02	3.73
CZTS-2	0.04	6.42
CZTS-3	0.06	13.56
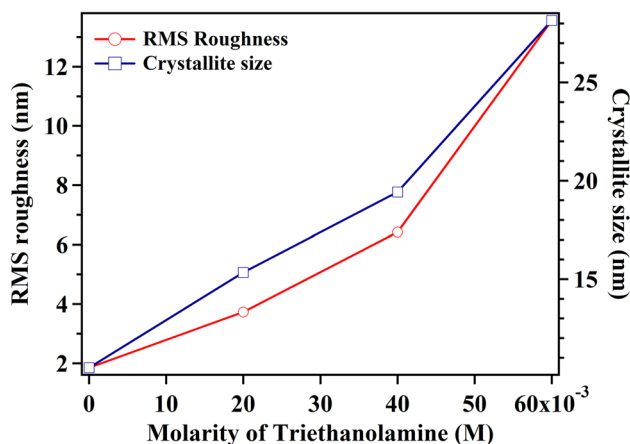
Fig. 5 RMS roughness of CZTS thin films deposited with various concentrations of TEA

in CZTS thin films at higher concentration of complexing agent. Our surface structural study lead to the conclusion that optimized concentration of complexing agent TEA has beneficial effects on growth of CZTS thin films for photovoltaic application.

Figure 6 displays surface and cross-sectional FE-SEM images of the CZTS-0 (a) and CZTS-3 (b) thin films. Figure 6a shows top view of CZTS-0 thin film consist of smooth, crack-free nano sized CZTS garin with excellent homogeneity. The cross-sectional image Fig. 6a shows complete crystallization of the CZTS thin film and thickness of

CZTS-0 thin film is 0.731 μm. Figure 6b shows surface view of CZTS-3 thin film which indicates that CZTS thin film is uniform, homogeneous, crack-free and pinhole-free surface with nanocrystal structure. The CZTS grain size increases notably and is more uniform compared with that obtain in absence of complexing agent. The cross-sectional image Fig. 6b shows CZTS-3 thin films contains densely packed CZTS grains with thickness 0.738 μm.

3.4 XPS measurement

To confirm atomic multivalancy in sol–gel processed CZTS film with the concentration of TEA of 0.06 M, XPS was employed. High-resolution core level spectra were recorded for Cu 2p region, Zn 2p region, Sn 3d region and S 2p region to determine valance states of cation in CZTS film. Figure 7a shows the Cu 2p XPS spectrum for CZTS thin film; it can be observed that the binding energy values for Cu 2$p_{3/2}$ and Cu 2$p_{1/2}$ are at 931.37 and 950.96 eV respectively, with peak splitting of 19.59. Therefore, it can be concluded that copper is in +1 oxidation state, suggesting Cu in CZTS film is in Cu$^+$ oxidation state, indicating that Cu^{2+} is reduced during the process of ionic reaction [38, 39]. Figure 7b demonstrates XPS spectrum of Zn 2p core level spectrum with binding energy peaks located at 1020.81 and 1043.75 eV respectively, corresponds to Zn 2$p_{3/2}$ and Zn 2$p_{1/2}$, with peak separation of 22.94 eV, which are in agreement with standard value 22.97 eV [38], suggesting Zn is present in Zn^{2+} oxidation state [38, 39]. Figure 7c represents XPS spectrum of Sn 3d core level suggesting that Sn 3$d_{5/2}$ and 3$d_{3/2}$ peaks are located at 486.52 and 494.96 eV respectively and a peak separation of 8.44 eV suggesting that Sn atom is present in CZTS thin film is in Sn^{4+} oxidation state [38, 39]. Figure 7d indicates XPS spectrum of S 2p core level spectrum with binding energy peaks located at 161.22 and 162.23 eV, respectively, with peak splitting of 1.01 eV, which are in agreement with the 160–164 eV range expected for S in sulfide phase in CZTS thin film [38, 39]. Analysis of XPS spectra clearly suggests that the atomic ratios of the cations and sulfides are in good agreement with the stoichiometric
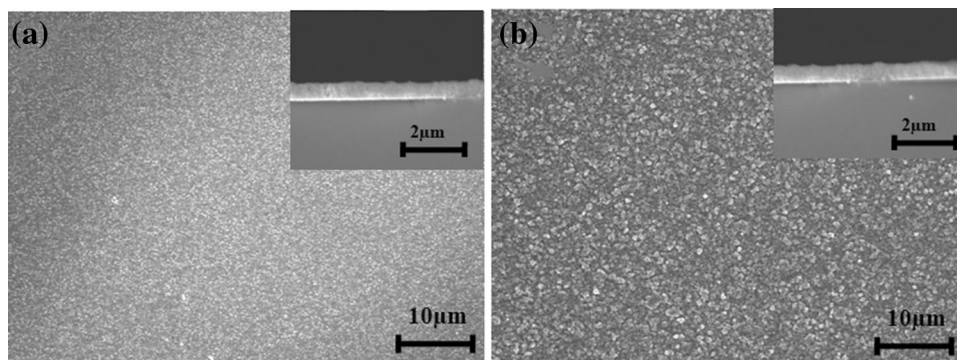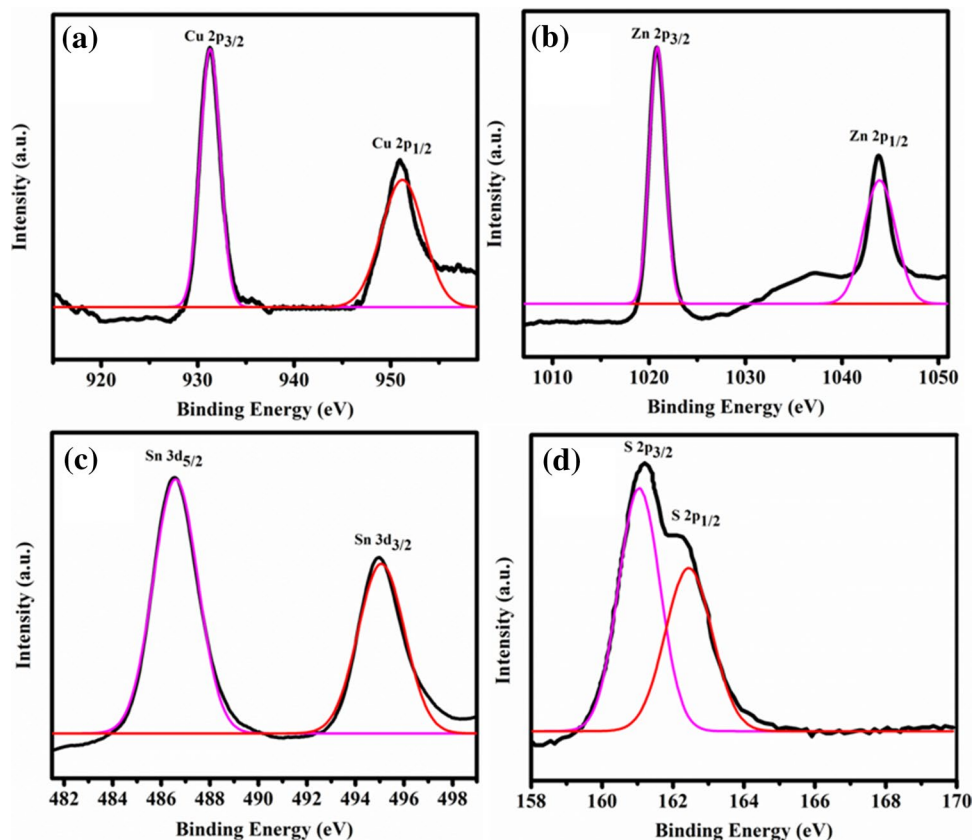
Fig. 6 Top view FE-SEM images of CZTS thin film samples: **a** CZTS-0, **b** CZTS-3: insets show cross-sectional images

Fig. 7 High resolution XPS spectra of **a** Cu 2*p*, **b** Zn 2*p*, **c** Sn 3*d* and **d** S 2*p* core levels of CZTS-3 thin film

CZTS film. No shoulder-peaks have been observed for any spectra which confirmed that guest atom has not incorporated in CZTS thin film.

3.5 Electrical and photovoltaic properties

In order to analyze the electronic transport in the CZTS thin films, Hall measurement was performed using the Van der Pauw geometry at room temperature. Hall coefficient of all CZTS thin films was found to be positive, suggesting p-type conductivity in CZTS films. The plot of resistivity and carrier concentration of CZTS thin films as a function of the concentration of complexing agent is shown in Fig. 8. The maximum resistivity was found to be for CZTS-0 film and it is of 254.3 Ω cm and minimum resistivity of 6.15 Ω cm is observed for CZTS-3 film. It is seen that the resistivity of CZTS thin films notably decreasing with increasing concentration of complexing agent, on the other hand, the carrier concentrations in CZTS thin films were found to increase almost in the same fashion (Fig. 8). The decrease in the film resistivity is due to increase in the grains size in CZTS thin film. The growth in grains of CZTS thin film leads to reduction in GB scattering due to charge carriers [40, 41], thus resistivity of the CZTS films decreases with increasing concentration of complexing agent [34]. The values of resistivity and carrier concentration are in good agreement
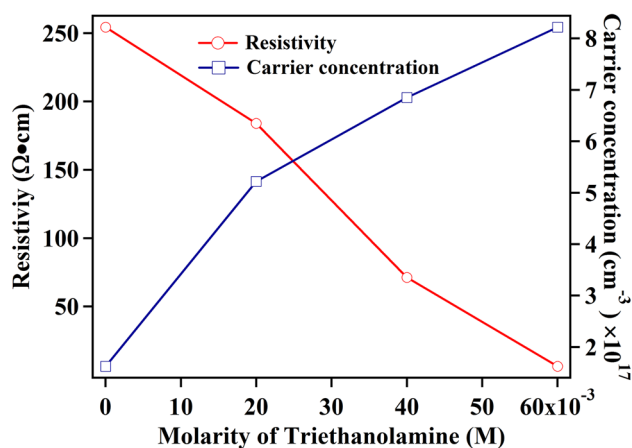

Fig. 8 Resistivity and Carrier concentration of CZTS thin films deposited with various concentations of TEA

with previously reported values [42]. The influence of TEA concentration on electrical properties of CZTS thin films is summarised in Table 3. These findings again emphasise on the positive role of complexing agent as a most favourable complexing agent for CZTS film growth for solar cell applications.

In order to examine quality of CZTS thin films for CZTS thin films solar cells, we have fabricated CZTS TFSC with

Table 3 Resistivity and carrier concentration of CZTS thin films deposited with different concentration of TEA

Sample name	Concentration of TEA (M)	Resistivity (Ω cm)	Carrier concentration (cm^{-3})
CZTS-0	0	254.3	1.624×10^{17}
CZTS-1	0.02	183.9	5.219×10^{17}
CZTS-2	0.04	71.2	6.851×10^{17}
CZTS-3	0.06	6.15	8.216×10^{17}
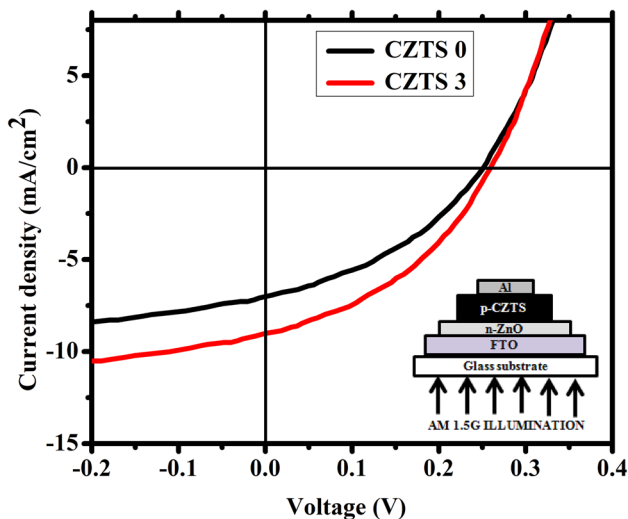
Fig. 9 *J–V* characteristic curve of CZTS TFSC under dark and illumination condition (AM 1.5 G spectrum and power density of 100 mW/cm). Inset shows schematic device architecture

the structure of SLG/FTO/ZnO/CZTS/Al. In our standard process ZnO layer was deposited on FTO coated glass substrate (sheet resistance is 20 Ω/sq) by spin coater at 3000 rpm for 30 s. The precursor solution was prepared by dissolving zinc acetate $C_4H_6O_4Zn$ (0.1 M) in 10 ml 2-methoxyethanol. The precursor layer was then pre-annealed on a hot plate at 300 °C for 10 min. The process of coating and drying of ZnO thin films were repeated four times to obtain ZnO thin film of desired film thickness followed by annealing the films at 480 °C for 1.5 h in air. Aluminium circular electrodes of 2 mm diameter were deposited on CZTS absorber layer via thermal evaporation method to make back contact electrodes of TFSCs devices. The active area of CZTS TFSCs was 0.16 cm^2. Figure 9 shows current

density–voltage characteristics (*J–V*) curve of solar cells of an active area of 0.16 cm^2 measured under AM 1.5 (1000 W/m^2) illumination. Photovoltaic performance of CZTS TFSCs with a simulated AM 1.5 G spectrum and power density of 100 mW/cm^2 at 25 °C is shown in Table 4. Further optimization in the efficiency of CZTS TFSCs could be made by increasing thickness of the CZTS layer, which would definitely lead to increase in J_{sc} and hence efficiency of CZTS TFSCs could be increased.

4 Conclusion

Kesterite CZTS thin films for absorber layer of solar cells have been prepared by a simple sol–gel process without sulphurization with different amount of TEA as a complexing agent. The crystallinity of CZTS thin films enhances with optimized concentration of TEA. XRD and Raman spectra studies reveal that CZTS thin films have polycrystalline kesterite crystal structure and optimized concentration of TEA promotes single phase kesterite structure and phase purity of CZTS films. AFM study revealed highly uniform grains distribution and significant CZTS grain growth with the increase of the concentration of complexing agent TEA. Also, SEM analysis revealed that CZTS thin films were dense, crack-free and uniform. The study of optical properties demonstrates that CZTS films have direct optical band gaps. Moreover, energy band gap decreases from 1.78 to 1.50 eV as the concentration of complexing agent increases, which is ideal for solar energy conversion. Hall measurements revealed that electrical resistivity decreases and charge carrier concentration increases systematically as the concentration of complexing agent increases. Analysis of XPS spectra clearly suggests that the atomic ratios of the cations and sulfides are in good agreement with the stoichiometric CZTS film. Our results clearly suggest that optimized concentration of complexing agent TEA improves crystallinity and single phase kesterite structure in CZTS thin films without sulfurization process. CZTS TFSCs with a structure of SLG/FTO/ZnO/CZTS/Al were fabricated with about 0.87% conversion efficiency have been obtained using CZTS absorber with optimized TEA concentartion. Further optimization on annealing temperature, prevention of charge carrier loss, chemical composition and increasing CZTS absorber layer thickness are in progress to obtain highly efficient CZTS TFSCs.

Table 4 Photovoltaic performance of CZTS TFSCs with a simulated AM 1.5 G spectrum and power density of 100 mW/cm^2 at 25 ºC

Sample name	η (%)	V_{oc} (V)	J_{sc} (mA/cm^2)	Fill factor (%)	R_s (Ohm cm^2)	R_{sh} (Ohm cm^2)
CZTS-0	0.62	0.25	6.92	36	14.96	131.27
CZTS-3	0.87	0.257	8.95	38	9.72	264.41

Compliance with ethical standards

Conflict of interest The authors declare there is no conflict of interest.

References

1. M. Powalla, P. Jackson, D. Hariskos, W. Witte, R. Wurz, E. Lotter, R. Menner, W. Wischman, In *Proceedings of the 29th European Photovoltaic Solar Energy Conference 3AO 4.2*, Amsterdam, 2014
2. R.B.V. Chalapathy, G.S. Jung, B.T. Ahn, Sol. Energy Mater. Sol. Cells **95**, 3216–3221 (2011)
3. A.V. Moholkar, S.S. Shinde, A.R. Babar, K.U. Sim, H.K. Lee, K.Y. Rajpure, P.S. Patil, C.H. Bhosale, J.H. Kim, J. Alloys Compd. **509**, 7439–7446 (2011)
4. H. Katagiri, K. Jimbo, S. Yamada, T. Kamimura, W.S. Maw, T. Fukano, Appl. Phys. Express **1**, 041201–041202 (2008)
5. B.A. Schubert, B. Marsen, S. Cinque, T. Unold, R. Klenk, S. Schorr, Prog. Photovolt. Res. Appl. **19**, 93–96 (2011)
6. M. Jiang, Y. Li, R. Dhakal, P. Thapaliya, M. Mastro, J.D. Caldwell, F. Kub, X. Yan, J. Photon. Energy **01950**, 1–6 (2011)
7. K. Tanaka, M. Oonuki, N. Moritake, H. Uchiki, Sol. Energy Mater. Sol. Cells **93**, 583–587 (2009)
8. O.V. Galan, M. Courel, M.E. Rodriguez, D.J. Olarte, M.A. Frutis, E. Saucedo, Sol. Energy Mater. Sol. Cells **132**, 557–562 (2015)
9. H. Park, H. Young, Hwang, J. Sol-Gel Sci. Technol. **65**, 23–27 (2013)
10. T.K. Todorov, K.B. Reuter, D.B. Mitzi, Adv. Mater. **22**, E156–E159 (2010)
11. W. Ki, H.W. Hillhouse, Adv. Energy Mater. **1**, 732–735 (2011)
12. M.O. Loapez, A.M. Acevedo, Thin Solid Films **330**, 96–101 (1998)
13. T.K. Chaudhuri, D. Tiwari, Sol. Energy Mater. Sol. Cells **101**, 46–50 (2012)
14. B.D. Cullity, *Elements of X-Ray Diffraction*, vol. 2 (Addison–Wesley Publishing Company, Inc., Boston, 1956), pp. 99–256
15. A. Kassim, H.S. Min, T.W. Tee, N.C. Fei, Am. J. Appl. Sci. **8**, 359–361 (2011)
16. P.A. Fernandes, P.M.P. Salome, A.F. da Cunha, Thin Solid Films **517**, 2519–2523 (2009)
17. X. Fontane, L.C. Barrio, V.I. Roca, E. Saucedo, A.P. Rodriguez, J.R. Morante, D.M. Berg, P.J. Dale, S. Siebentritt, Appl. Phys. Lett. **98**, 181905 (2011)
18. T.H. Nguyen, W. Septina, S. Fujikawa, F. Jiang, T. Harada, S. Ikeda, RSC Adv. **5**, 77565–77571 (2015)
19. P.R. Ghediya, T.K. Chaudhuri, D. Vankhade, J. Alloys Compd. **685**, 498–506 (2016)
20. D.A. Skoog, F.J. Holler, S.R. Crouch, *Principles of Instrumental Analysis*, 6th edn. (Thomson Books Publisher, Belmont, 2007), pp. 481–491
21. P.R. Ghediya, T.K. Chaudhuri, J. Phys. D **48**, 455109 (2015). pp)
22. A.J. Cheng, M. Manno, A. Khare, C. Leighton, S.A. Campbell, E.S. Aydil, J. Vac. Sci. Technol. A **29**, 051203–051211 (2011)
23. M. Himmrich, H. Haeuseler, Spectrochim. Acta Mol. Biomol. Spectrosc. **47**, 933–942 (1991)
24. D. Dumcenco, Y.S. Huang, Opt. Mater. **35**, 419–425 (2013)
25. J. Tao, J. Liu, J. He, K. Zhang, J. Jiang, L. Sun, P. Yang, J. Chu, RSC Adv. **4**, 23977–23984 (2014)
26. P.A. Fernandes, P.M.P. Salome, A.F. da Cunha, Phys. Status Solidi C **7**, 901–904 (2010)
27. P.A. Fernandes, P.M.P. Salome, A.F. da Cunha, J. Phys. D **43**, 215403–215413 (2010)
28. J. Serrano, A. Cantarero, M. Cardona, N. Garro, R. Lauck, R.E. Tallman, T.M. Ritter, B.A. Weinstein, Phys. Rev. B **69**, 014301 (2004)
29. C.G. Munce, G.K. Parker, S.A. Holt, G.A. Hope, Colloids Surf. A **295**, 152–158 (2007)
30. S.P. Louise, P.P. Ivan, M.E.H. Amanda, C.J.H. Robin, Chem. Mater. **11**, 1792–1799 (1999)
31. Z. Seboui, A. Gassoumi, Y. Cuminal, N.K. Turki, Superlattices Microstruct. **75**, 586–592 (2014)
32. J. Tauc, in *Optical Properties of Solids*, ed. by F. Abeles (North-Holland Publishers, Amsterdam, 1972), pp. 277–279
33. J. Wang, P. Zhang, X. Song, L. Gao, RSC Adv. **4**, 21318–21324 (2014)
34. M. Oztas, Chin. Phys. Lett. **25**(11), 4090 (2008)
35. C.S. Kanurul, G.L. Shekar, L. Krishnamurthy, R.G.K. Urs, J. Nano- Electron. Phys. **6**(2), 02004 (2014)
36. S.Y. Lee, B.O. Park, Thin Solid Films **516**, 3862–3864 (2008)
37. Z. Li, J.C.W. Ho, K.K. Lee, X. Zeng, T. Zhang, L.H. Wong, Y.M. Lam, RSC Adv. **4**, 26888–26894 (2014)
38. G.L. Agawane, S.W. Shin, S.A. Vanalakar, M.P. Suryawanshi, A.V. Moholkar, J.H. Yun, J. Gwak, J.H. Kim, J. Mater. Sci.: Mater. Electron. **26**, 1900–1907 (2015)
39. J. Wang, P. Zhang, X. Song, L. Gao, RSC Adv. **5**, 1220–1226 (2015)
40. Q.G. Zhang, X. Zhang, B.Y. Cao, Appl. Phys. Lett. **89**, 114102 (2006)
41. K. Barmak, A. Darbal, K.J. Ganesh, P.J. Ferreira, J.M. Rickman, T. Sun, B. Yao, A.P. Warren, K.R. Coffey, J. Vac. Sci. Technol. A **32**, 061503 (2014)
42. M. Patel, I. Mukhopadhyay, A. Ray, J. Phys. D **45**, 445103 (2012)